

## Pressure-induced structural transformation of clathrate Ge<sub>136</sub> via ultrafast recrystallization of an amorphous intermediate

Marián Ryník,<sup>1,\*</sup> Stefano Leoni,<sup>2,†</sup> and Roman Martoňák<sup>1,‡</sup>

<sup>1</sup>*Department of Experimental Physics, Comenius University, Mlynská Dolina F2, 842 48 Bratislava, Slovakia*

<sup>2</sup>*School of Chemistry, Cardiff University, Cardiff, CF10 3AT, United Kingdom*



(Received 23 December 2021; revised 11 March 2022; accepted 1 April 2022; published 21 April 2022)

We study the pressure-induced structural transformation of Ge<sub>136</sub> clathrate by *ab initio* molecular dynamics and metadynamics. The system under pressure first undergoes amorphization followed by an ultrafast recrystallization to the  $\beta$ -tin structure on the time scale of 30 ps. The initial pressure-induced amorphization of clathrate is triggered by high pressure while the subsequent fast recrystallization to  $\beta$ -tin is driven by low temperature. Interestingly, the amorphous intermediate is still diffusive even at room temperature in spite of very strong undercooling, making the ultrafast recrystallization possible. The system provides an explicit example of structural transformation between two crystalline phases proceeding via noncrystalline intermediate. On fast decompression of the amorphous structure with incipient crystalline order, the recrystallization is blocked and the system instead proceeds to the tetrahedral low-density amorphous (LDA) phase.

DOI: [10.1103/PhysRevB.105.134107](https://doi.org/10.1103/PhysRevB.105.134107)

### I. INTRODUCTION

Open framework structures like clathrates [1–3] are enjoying a renewed interest because they may host distinct electronic, magnetic, spectral and transport properties [4–8]. Due to their low density, clathrates are thermodynamically metastable at ambient conditions and typically become stable only at negative pressures. It can therefore be expected that even on a modest compression they would readily transform to denser phases. It is less obvious, however, how a complicated order in a large unit cell containing  $\sim 10^2$  atoms could transform to standard crystalline phase with few atoms in the unit cell. Certainly it is difficult to imagine any kind of simple martensitic mechanism directly accomplishing such transformation.

Interesting examples are clathrates of group IV elements, in particular Si and Ge (for comparison of Si, Ge, and C clathrates, see Ref. [9]). The high-pressure behavior of filled clathrates was studied, e.g., for Ba<sub>8</sub>Si<sub>46</sub> [10], Ba<sub>7.5</sub>Si<sub>45</sub> [11], Ba<sub>8</sub>Ge<sub>43</sub> [12], or Rb<sub>6.15</sub>Si<sub>46</sub> [13], where pressure-induced amorphization (PIA) and polyamorphic transition were observed (for a review, see Refs. [14–16]). Type-II clathrate Ge(cF136) allotrope was synthesized from a salt precursor Na<sub>12</sub>Ge<sub>17</sub> by mild oxidation with HCl. It is stable at room condition and subsists up to 693 K [17]. Amorphous minority phases are encountered during Ge<sub>136</sub> synthesis [17]. We note that recently a new fabrication method for type-II Ge clathrate film was proposed in Ref. [18]. The pressure-induced structural changes and behavior of Ge<sub>136</sub> on compression were studied in Ref. [19] for a sample containing nearly 2% of

impurities, and several transformations into denser crystalline Ge phases (hR8, tI4) were found via compression above 7.6 GPa. No such study is known for guest-free Ge<sub>136</sub>. In high-pressure studies of guest-free Si<sub>136</sub> clathrate [3,20], the system was found to transform at a pressure of 8–10 GPa to the 6-coordinated  $\beta$ -tin structure. Thermodynamically, it was found from DFT calculations that the  $\beta$ -tin structure becomes more stable with respect to the Si<sub>136</sub> clathrate already at a pressure of 3–4 GPa [20]. The need for substantial overpressurization was attributed to the absence of a convenient low-energy pathway for the Si<sub>136</sub> to  $\beta$ -tin transition.

Here we focus on the pressure-induced transformations of Ge<sub>136</sub> and study them by means of *ab initio* simulations. The phase diagrams of Si and Ge are very similar, but the range of stability of the  $\beta$ -tin phase in Ge is much wider than in Si [21]. The aim of our study is twofold: Find a theoretical prediction for the high-pressure behavior of Ge<sub>136</sub> clathrate and uncover the elusive microscopic mechanism of the transformation.

### II. COMPUTATIONAL METHODS

We employ *ab initio* molecular dynamics (MD) and the metadynamics-based algorithm for simulation of structural phase transitions in crystals [22–24]. Metadynamics allows to overcome the free-energy barriers and avoid the use of excessive overpressurization typically encountered in plain MD simulations of structural transformations in solids (for a review see Refs. [25–28]; references to applications of the method can be found within the recent work [29]). *Ab initio* calculations were performed by the VASP code [30,31] employing PBE functional [32], standard PAW pseudopotential with four valence electrons, and plane-wave kinetic energy cutoff of 226 eV. MD was performed with  $2 \times 2 \times 2$  Monkhorst-Pack mesh of  $k$  points [33] and a time step of 2 fs. In NPT MD the barostat mass was set to 5000 a.u.

\*marian.rynik@fmph.uniba.sk

†leonis@cardiff.ac.uk

‡martonak@fmph.uniba.sk

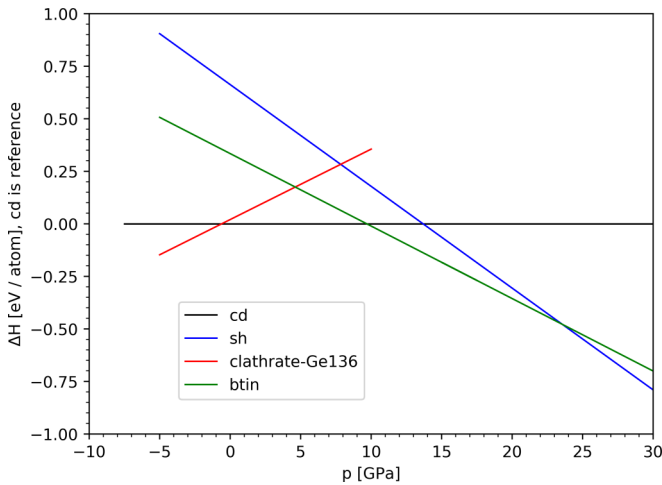


FIG. 1. Enthalpy (relative to the cubic diamond phase) as a function of pressure for the  $\text{Ge}_{136}$  clathrate, cubic diamond (cd),  $\beta$ -tin (bt), and simple hexagonal (sh) phases.

Metadynamics simulations were performed by means of 0.5 ps NVT runs (250 MD steps) and the Gaussian width and height were set to 60 (kbar  $\text{\AA}^3$ ) $^{1/2}$  and 3600 kbar  $\text{\AA}^3 = 2.25$  eV (representing 16.5 meV/atom), respectively. The simulation cell was formed by a single unit cell of  $\text{Ge}_{136}$ .

### III. RESULTS AND DISCUSSION

The enthalpies of the  $\text{Ge}_{136}$  clathrate, cubic diamond,  $\beta$ -tin, and simple hexagonal structure are shown in Fig. 1 where it can be seen that the  $\beta$ -tin structure becomes more stable with respect to clathrate at 4 GPa. In order to assess the ultimate structural stability of the clathrate on compression, we started with static compression at  $T = 0$ , increasing pressure in 5 GPa steps. Clathrate survived up to 30 GPa while at 35 GPa it reached a limit of mechanical stability and quickly transformed into a 6-coordinated disordered structure. The evolution of structure during 200 geometry optimization steps is shown in Fig. 1 (see Supplemental Material [34]). Interestingly, in the initial phase of the collapse the structure stratifies into (111) layers of coordination 4 and 5. The final disordered structure has a radial distribution function (RDF) which is remarkably structureless in the region from 3 to 4.5  $\text{\AA}$  (Fig. 2(a); see Supplemental Material [34]). The angular distribution function (ADF) (Fig. 2(b); see Supplemental Material [34]) has a sharp peak at 60° and for higher angles is nearly flat up to 130° where it starts to drop, also pointing to substantial disorder.

In order to make sure that the PIA observed at  $T = 0$  is not just an artifact of overpressurization, we performed *ab initio* metadynamics employing the cell as collective variable [24] at a lower pressure of 10 GPa and  $T = 300$  K. At finite temperature the system is able to cross the barriers and one can expect the structural transformation to start at a lower pressure, possibly resulting in different and more ordered structure.

The evolution of structure and energy of the clathrate is shown in Fig. 2(a). During the first 76 metasteps (19,000 MD steps) the enthalpy of the system gradually grows while

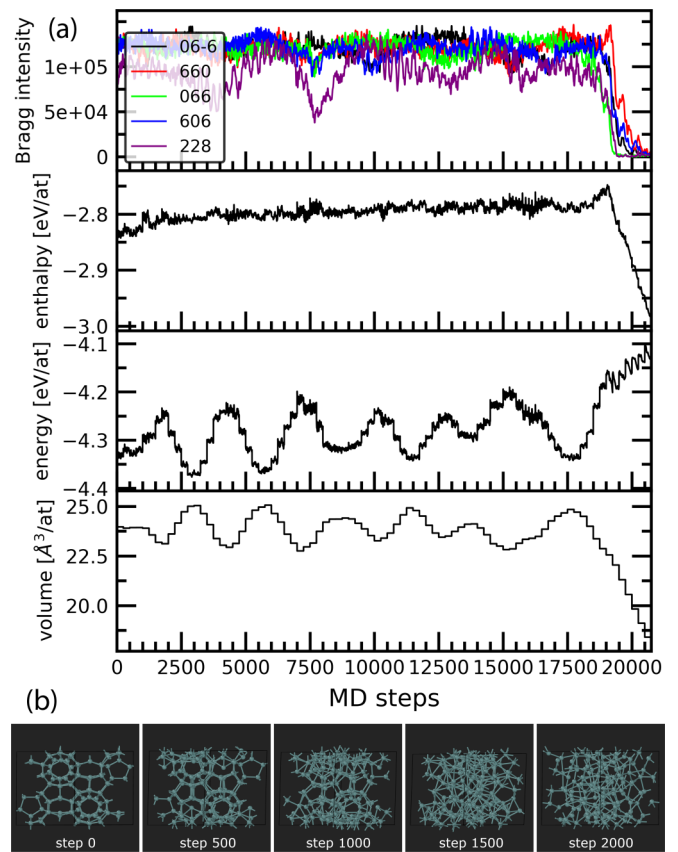


FIG. 2. (a) Upper panel: Time evolution of volume, energy, enthalpy, and intensity of selected Bragg peaks of clathrate structure in metadynamics at  $p = 10$  GPa and  $T = 300$  K, resulting in the amorphization of  $\text{Ge}_{136}$  clathrate after 83 metasteps. (b) Lower panel: Sequence of configurations from metadynamics steps 76–83 (2000 MD steps from 18750 to 20750) where the PIA of clathrate occurs. The figure was prepared using the OVITO package [35].

the volume, energy, and intensity of Bragg peaks oscillate as the system explores the initial free-energy basin. After 76 metasteps the clathrate structure starts to collapse, signaled by vanishing of the Bragg peaks. The collapse is accomplished at metastep 83, accompanied by a large volume drop of about 25% and an enthalpy drop of 0.16 eV/atom. The collapse again produces a disordered structure (see the structural evolution in Fig. 2(b)) with very similar RDF (Fig. 3) as the structure produced at  $T = 0$  (Fig. 2(a); see Supplemental Material [34]). Metadynamics simulation of room-temperature compression thus confirms the PIA scenario found at  $T = 0$ . We note that the temperature during the structural transformation is well controlled by the thermostat (Fig. 3; see Supplemental Material [34]).

Performing metadynamics further after the collapse of the clathrate is not justified since for the noncrystalline disordered phase the supercell edges no longer represent good collective variables, and unphysical changes of the shape of the system might occur. Therefore in order to further follow the evolution of the disordered system, we switched off the Gaussians after metastep 83 and performed plain NPT MD for another 20,000 steps (40 ps). Surprisingly, we observed a recrystallization of the disordered phase. Such ultrafast recrystallization observed in a short *ab initio* MD run at room temperature appears rather

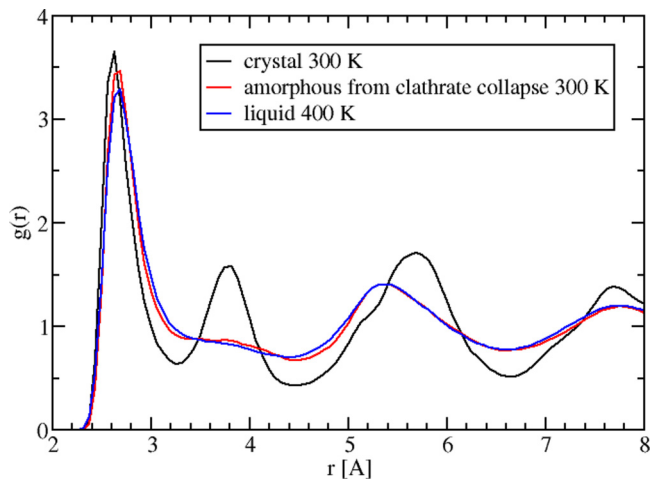


FIG. 3. RDF of the system in disordered and crystalline state at  $p = 10$  GPa and various temperatures.

unusual. The evolution of the volume, energy, enthalpy, and intensity of selected Bragg peaks is shown in Fig. 4(a). During the first 12,000 steps the enthalpy slowly decreases while some Bragg peaks slowly grow. Afterward the peaks start to grow very fast, enthalpy drops, and a defective  $\beta$ -tin phase is formed. After 17,000 steps the latter phase transforms into defective simple hexagonal phase. This last transformation is likely to be related to the presence of defects since the

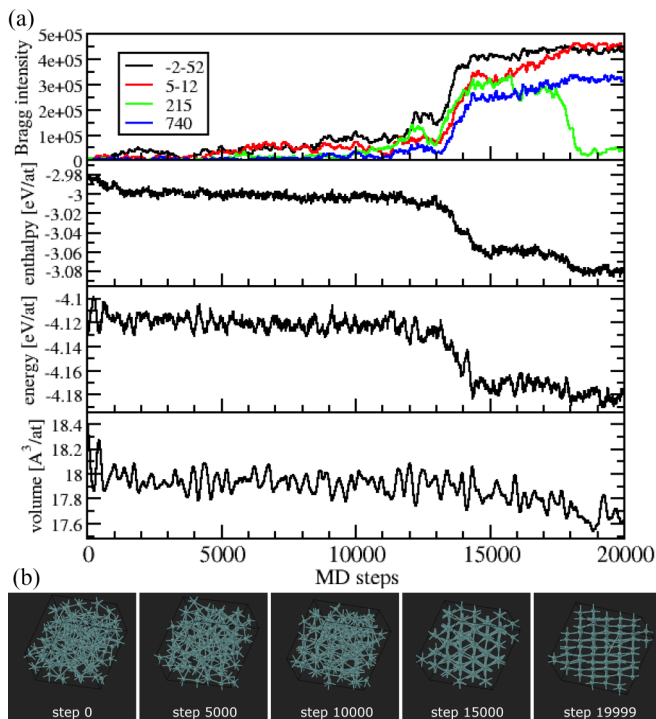


FIG. 4. (a) Upper panel: Time evolution of volume, energy, enthalpy, and intensity of selected Bragg peaks during NPT MD after amorphization of  $\text{Ge}_{136}$  at  $p = 10$  GPa and  $T = 300$  K. (b) Lower panel: Structural evolution of the system during the recrystallization of the amorphous phase. The figure was prepared using the OVITO package [35].

ideal sh phase becomes thermodynamically stable only at a higher pressure (see Fig. 1). We note that one cannot expect a formation of a perfect crystal since the number of atoms in the supercell is 136 which does not allow creation of a perfect supercell with edges being small integer multiples of unit cell vectors of crystalline phases. The structural evolution of the system and the formation of crystalline order from the amorphous phase are shown in Fig. 4(b) and Fig. 4 (see Supplemental Material [34]).

The observed PIA of the clathrate has features analogous to the “cold melting” suggested to operate, e.g., in PIA of water ice resulting in the HDA phase [36,37]. The melting line of the cubic diamond phase has a negative Clapeyron slope and the melting temperature reaches a minimum of 800 K at a pressure of 10 GPa [21]. Because of a lack of a mechanism allowing a direct transformation of the clathrate to another crystalline phase, the existence of a low free-energy supercooled liquid offers a kinetic route toward a disordered structure available on compression of the clathrate, providing a rationale for the PIA. Within this scenario the disordered phase prepared by PIA of the clathrate should have the same structure and exhibit the same ultrafast recrystallization behavior as the supercooled liquid obtained by fast cooling of liquid at the same pressure. Interestingly, a similarly fast recrystallization was recently described in very high-density amorphous (VHDA) Si [38]. It was not, however, observed in computational studies of Ge which focused on the low-density amorphous (LDA)/high-density amorphous (HDA) transition [39,40].

To test this hypothesis we melted the final recrystallized structure by heating it to 1000 K at 10 GPa over 20 ps. The liquid phase was subsequently quickly cooled down to 800 to 600 to 500 to 400 to 300 K, performing at each temperature a 20–40 ps MD run. The liquid phase persisted down to 300 K where the system again rapidly recrystallized within 20 ps as can be seen on the enthalpy evolution in Fig. 5(a), similarly to the crystallization after clathrate collapse. The same crystallization also occurred at  $T = 400$  K within an extended run of additional 40 ps [inset of Fig. 5(a)]. Interestingly, the RDF of the amorphous phase from clathrate collapse at 300 K is also very similar to that of the liquid before crystallization at 400 K (Fig. 3). A remarkable feature of both RDFs is the lack of the peak corresponding to the second coordination shell of the crystal at 3.8 Å (Fig. 3). The pressure-induced collapse of the clathrate structure therefore produces an amorphous phase which is structurally very similar to the one obtained by fast liquid cooling. Importantly, both structures appear equally prone to ultrafast crystallization. We note that in order to crystallize quickly the supercooled liquid must still have sufficient diffusivity. We therefore monitored the mean-squared displacement of the atoms at different temperatures which is shown in Fig. 5(b). It can be seen that the liquid even when cooled down to 300 K does not represent a frozen glass where atoms merely vibrate around their average positions. The glass transition temperature must therefore be rather low, allowing the system to crystallize before it freezes to amorphous solid. This appears to be a rather unusual property of the supercooled liquid Ge under pressure.

The observed ultrafast recrystallization points to the lack of barrier separating the disordered and the crystalline phase.

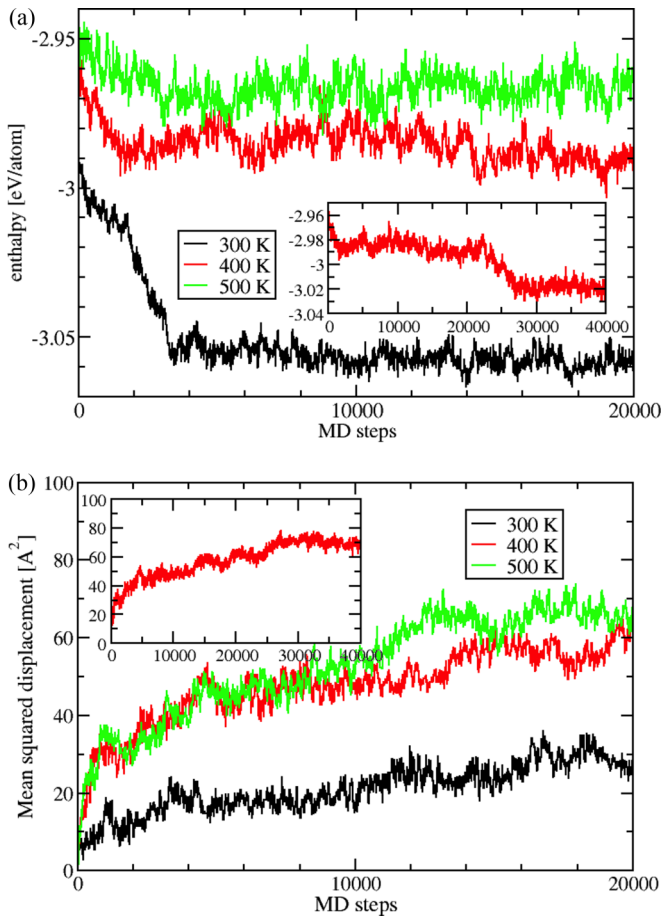


FIG. 5. Enthalpy evolution (a) (upper panel) and mean-squared displacement of atoms (b) (lower panel) during liquid cooling over 20,000 MD steps at  $p = 10$  GPa and  $T = 500, 400, 300$  K. Crystallization starts at  $T = 300$  K after 4000 steps. The inset shows an extended run over a total of 40,000 MD steps at  $T = 400$  K where the system also crystallized after 27,000 steps.

The crystallization in a strongly supercooled yet diffusive liquid thus occurs due to the loss of stability of the supercooled liquid. The whole process of transformation of the clathrate to the  $\beta$ -tin therefore represents a sequence of two off-equilibrium processes occurring in the respective metastable parent phases. The initial PIA of clathrate is triggered by high pressure while the subsequent fast recrystallization to  $\beta$ -tin is driven by low temperature.

Finally, we studied whether the ultrafast recrystallization of the dense amorphous phase also persists to lower pressures. To this end we repeated metadynamics simulation of the clathrate at a lower pressure of 5 GPa where the amorphization occurred after 278 metasteps. The resulting amorphous phase already exhibited an incipient crystalline order as can be seen on the RDF in Fig. 6(b) where a small peak appears at the position of the second coordination shell at 3.9 Å. Afterward we followed the structural evolution at even lower pressures, suddenly decompressing the phase from 5 GPa directly to pressures of 3, 2, 1.5, 1.25, 1.1, and 1 GPa. Interestingly, we found a boundary between two manifestly different regimes. The evolution of the system in the E-V plane is shown in Fig. 6(a). It is seen that at pressures down to 1.25 GPa the sys-

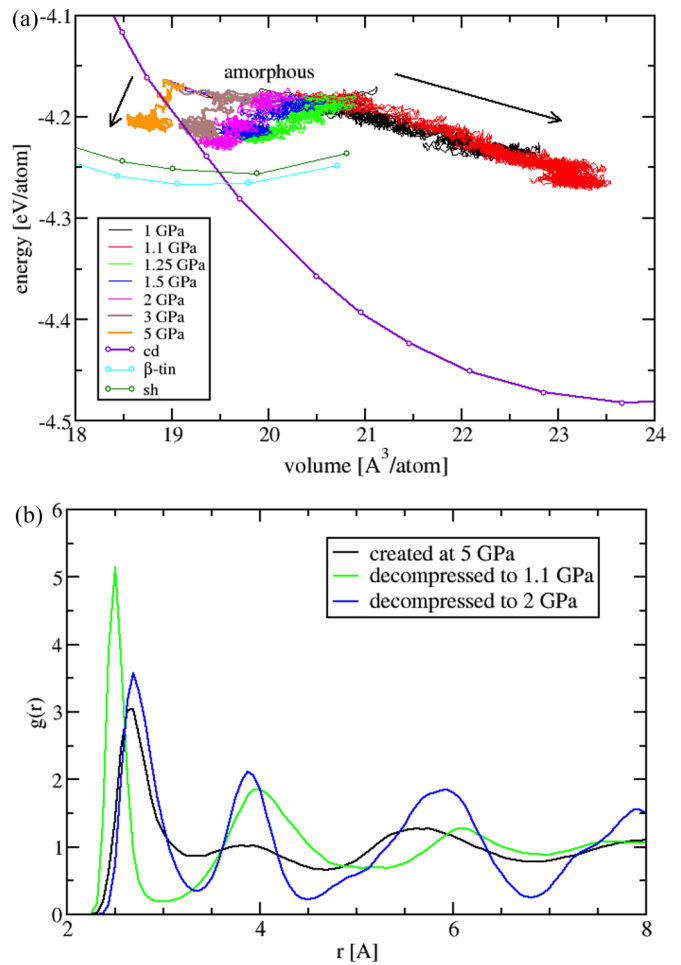


FIG. 6. (a) Upper panel: Energy vs volume after sudden decompression of amorphous Ge prepared by compression of the clathrate  $\text{Ge}_{136}$  at 5 GPa and 300 K. Arrows show the different directions of the evolution in the two regimes. (b) Lower panel: RDF of the amorphous phase with incipient crystalline order at 5 GPa as well as of the phases after decompression to 2 and 1.1 GPa, showing different structural evolution.

tem still approaches the E-V curves of the  $\beta$ -tin and sh phases (and eventually crystallizes). For decompression to 2 GPa this is demonstrated also in Fig. 6(b) where the initially small peak at 3.9 Å grows to a full peak of the crystalline phase while the volume shrinks [Fig. 6(a)]. On the other hand, the evolution of the RDF after decompression to 1.1 GPa is very different—the system strongly expands its volume [Fig. 6(a)] and RDF evolves toward different peaks, where notably the first peak moves toward shorter bond. The different evolution pattern is also very clearly seen on the time evolution of the ADF shown for both cases in Fig. 5 (see Supplemental Material [34]). In this regime, interestingly, the sudden expansion of the phase with incipient crystalline order drives the system to a disordered state followed by structural arrest, resulting in the tetrahedral amorphous LDA phase. We note that the energy of the amorphous phase created by clathrate amorphization is only slightly above ( $\sim 0.07$  eV) that of the  $\beta$ -tin and sh crystalline phases, indicating that the energy landscape of the relevant megabasin is rather flat [Fig. 6(a)]. This is

also consistent with the lower barriers toward crystallization. On the other hand, the energy of the LDA phase at lower pressures remains much higher ( $\sim 0.2$  eV) above the cubic diamond phase, consistent with much more structured energy landscape and a higher barrier making recrystallization much more difficult.

#### IV. CONCLUSIONS

The above observations suggest that the potential energy landscape (PES) of the disordered/liquid HDA phase is rather flat (unlike that of the low-pressure tetrahedral LDA Ge). This is compatible with the observed structural properties, namely, a nearly structureless RDF from 3 to 5 Å and a broad distribution of bond angles. This lack of roughness of the PES is also consistent with the low glass transition temperature, implying nonvanishing diffusivity even at low temperatures which eventually makes the ultrafast crystallization possible.

To conclude, we showed that the complex structure of clathrate Ge<sub>136</sub> on compression at room temperature transforms to the simple  $\beta$ -tin phase via a disordered phase with unusual properties. It thus provides an explicit example of structural transformation between two crystalline phases proceeding via noncrystalline intermediate. To further understand this interesting phenomenon it would be useful to perform the experiment at different temperatures. While the PIA can be expected to occur at all temperatures, the recrystallization

is likely to be temperature dependent. Our prediction for the final phase is the following: Above the melting temperature  $T_m$  (800 K), compression will melt clathrate; between  $T_m$  and the glass transition temperature  $T_g$ , compression will result in  $\beta$ -tin recrystallized from supercooled liquid; and finally, at sufficiently low temperature below  $T_g$ , compression will create a metastable HDA amorphous phase. It might also be possible to monitor the time evolution of the structure across the transition experimentally and to directly detect the presence of the amorphous intermediate, e.g., by means of femtosecond x-ray diffraction [41].

#### ACKNOWLEDGMENTS

M.R. and R.M. were supported by the VEGA Project No. 1/0640/20 and by the Slovak Research and Development Agency under Contract No. APVV-19-0371. The calculations were performed in the Computing Centre of the Slovak Academy of Sciences using the supercomputing infrastructure acquired in project ITMS 26230120002 and 26210120002 (Slovak infrastructure for high-performance computing) supported by the Research & Development Operational Programme funded by the ERDF. Part of calculations was performed on the GPU TITAN V provided by the NVIDIA grant. S.L. thanks the Leverhulme Trust for support under Project No. RPG-2020-052, as well as ARCCA Cardiff for computational support.

- 
- [1] C. Cros, M. Pouchard, and P. Hagemuller, *J. Solid State Chem.* **2**, 570 (1970).
- [2] J. S. Kasper, P. Hagemuller, M. Pouchard, and C. Cros, *Science* **150**, 1713 (1965).
- [3] A. San-Miguel, P. K  gh  lian, X. Blase, P. M  linon, A. Perez, J. P. Iti  , A. Polian, E. Reny, C. Cros, and M. Pouchard, *Phys. Rev. Lett.* **83**, 5290 (1999).
- [4] P. Melinon, P. K  gh  lian, X. Blase, J. Le Brusca, A. Perez, E. Reny, C. Cros, and M. Pouchard, *Phys. Rev. B* **58**, 12590 (1998).
- [5] A. A. Demkov, W. Windl, and O. F. Sankey, *Phys. Rev. B* **53**, 11288 (1996).
- [6] S. Saito and A. Oshiyama, *Phys. Rev. B* **51**, 2628 (1995).
- [7] R. Nesper, K. Vogel, and P. E. Bl  chl, *Angew. Chem., Int. Ed. Engl.* **32**, 701 (1993).
- [8] M. O'Keeffe, G. B. Adams, and O. F. Sankey, *Phys. Rev. Lett.* **68**, 2325 (1992).
- [9] D. Conn  table, *Phys. Rev. B* **82**, 075209 (2010).
- [10] A. S. Miguel, A. Merlen, P. Toulemonde, T. Kume, S. L. Floch, A. Aouizerat, S. Pascarelli, G. Aquilanti, O. Mathon, T. L. Bihan, J.-P. Iti  , and S. Yamanaka, *Europhys. Lett.* **69**, 556 (2005).
- [11] R. Debord, H. Euchner, V. Pischedda, M. Hanfland, A. San-Miguel, P. M  linon, S. Pailh  s, and D. Machon, *Acta Mater.* **210**, 116824 (2021).
- [12] T. Fukushima, T. Kume, S. Sasaki, H. Shimizu, H. Fukuoka, and S. Yamanaka, *Phys. Status Solidi B* **244**, 392 (2007).
- [13] D. Machon, P. Toulemonde, P. F. McMillan, M. Amboage, A. Mu  noz, P. Rodr  guez-Hern  ndez, and A. San Miguel, *Phys. Rev. B* **79**, 184101 (2009).
- [14] A. San-Miguel and P. Toulemonde, *High Press. Res.* **25**, 159 (2005).
- [15] P. Toulemonde, A. S. Miguel, A. Merlen, R. Viennois, S. L. Floch, C. Adessi, X. Blase, and J. Tholence, *J. Phys. Chem. Solids* **67**, 1117 (2006), Proceedings of the 13th International Symposium on Intercalation Compounds, Clermont-Ferrand, France, 6–9 June, 2005.
- [16] D. Machon, P. F. McMillan, A. San-Miguel, P. Barnes, and P. T. Hutchins, Semiconductor clathrates: In situ studies of their high pressure, variable temperature and synthesis behavior, in Nolas G. (eds), *The Physics and Chemistry of Inorganic Clathrates*, Springer Series in Materials Science, Vol. 199 (Springer, Dordrecht, 2014), Chap. 4, pp. 91–123
- [17] A. M. Guloy, R. Ramlau, Z. Tang, W. Schnelle, M. Baitinger, and Y. Grin, *Nature (London)* **443**, 320 (2006).
- [18] R. Kumar, Y. Hazama, F. Ohashi, H. S. Jha, and T. Kume, *Thin Solid Films* **734**, 138859 (2021).
- [19] U. Schwarz, A. Wosylus, B. B  hme, M. Baitinger, M. Hanfland, and Y. Grin, *Angew. Chem., Int. Ed.* **47**, 6790 (2008).
- [20] G. K. Ramachandran, P. F. McMillan, S. K. Deb, M. Somayazulu, J. Gryko, J. Dong, and O. F. Sankey, *J. Phys.: Condens. Matter* **12**, 4013 (2000).
- [21] L. C. Kelsall, M. Pe  a-Alvarez, M. Martinez-Canales, J. Binns, C. J. Pickard, P. Dalladay-Simpson, R. T. Howie, and E. Gregoryanz, *J. Chem. Phys.* **154**, 174702 (2021).
- [22] A. Laio and M. Parrinello, *Proc. Natl. Acad. Sci. USA* **99**, 12562 (2002).
- [23] R. Marto  n  k, A. Laio, and M. Parrinello, *Phys. Rev. Lett.* **90**, 075503 (2003).

- [24] R. Martoňák, D. Donadio, A. R. Oganov, and M. Parrinello, *Nat. Mater.* **5**, 623 (2006).
- [25] R. Martoňák, A. Laio, M. Bernasconi, C. Ceriani, P. Raiteri, F. Zipoli, and M. Parrinello, *Z. Kristallogr. - Cryst. Mater.* **220**, 489 (2005).
- [26] R. Martoňák, A. R. Oganov, and C. W. Glass, *Phase Transitions* **80**, 277 (2007).
- [27] R. Martoňák, *Eur. Phys. J. B* **79**, 241 (2011).
- [28] R. Martoňák, Simulation of structural phase transitions in crystals: The metadynamics approach, in *Modern Methods of Crystal Structure Prediction*, edited by A. R. Oganov (Wiley, New York, 2010), Chap. 5, pp. 107–130, <https://onlinelibrary.wiley.com/doi/pdf/10.1002/9783527632831.ch5>.
- [29] M. Badin and R. Martoňák, *Phys. Rev. Lett.* **127**, 105701 (2021).
- [30] G. Kresse and J. Furthmüller, *Phys. Rev. B* **54**, 11169 (1996).
- [31] G. Kresse and D. Joubert, *Phys. Rev. B* **59**, 1758 (1999).
- [32] J. P. Perdew, K. Burke, and M. Ernzerhof, *Phys. Rev. Lett.* **77**, 3865 (1996).
- [33] H. J. Monkhorst and J. D. Pack, *Phys. Rev. B* **13**, 5188 (1976).
- [34] See Supplemental Material at <http://link.aps.org/supplemental/10.1103/PhysRevB.105.134107> for additional graphs and figures, which includes Refs. [42,43].
- [35] A. Stukowski, *Modell. Simul. Mater. Sci. Eng.* **18**, 015012 (2010).
- [36] O. Mishima, L. D. Calvert, and E. Whalley, *Nature (London)* **310**, 393 (1984).
- [37] D. Machon, F. Meersman, M. Wilding, M. Wilson, and P. McMillan, *Prog. Mater. Sci.* **61**, 216 (2014).
- [38] V. L. Deringer, N. Bernstein, G. Csányi, C. B. Mahmoud, M. Ceriotti, M. Wilson, D. A. Drabold, and S. R. Elliott, *Nature (London)* **589**, 59 (2021).
- [39] M. Durandurdu and D. A. Drabold, *Phys. Rev. B* **66**, 041201 (2002).
- [40] G. Mancini, M. Celino, F. Iesari, and A. D. Cicco, *J. Phys.: Condens. Matter* **28**, 015401 (2016).
- [41] J. S. Wark, M. I. McMahan, and J. H. Eggert, Femtosecond diffraction and dynamic high pressure science, [arXiv:2203.02545](https://arxiv.org/abs/2203.02545) [cond-mat.other] (2022).
- [42] S. Le Roux and P. Jund, *Comput. Mater. Sci.* **49**, 70 (2010).
- [43] Plotly Technologies Inc., Montreal, QC, Collaborative data science (2015), <https://plot.ly>.